DOI: 10.1021/ic8018937

Inorganic Chemistry
Article

Syntheses, X-ray Structures, and Physicochemical Properties of Phenoxo-Bridged Dinuclear Nickel(II) Complexes: Kinetics of Transesterification of 2-Hydroxypropyl-*p*-nitrophenylphosphate

Sukanta Mandal,[†] V. Balamurugan,[†] Francesc Lloret,[‡] and Rabindranath Mukherjee*,[†]

[†]*Department of Chemistry, Indian Institute of Technology Kanpur, Kanpur 208 016, India, and* [‡]*Departament de Química Inorgànica/Instituto de Ciencia Molecular (ICMOL), Universitat de València, Polígono de la Coma, s/n, 46980-Paterna (València), Spain*

Received October 4, 2008

Four dinuclear nickel(II) complexes $[Ni^{II}_2(L^1)(O_2CMe)_2(H_2O)_2][PF_6]\cdot MeOH\cdot 3H_2O$ (**1**), $[Ni^{II}_2(L^1)(O_2CMe)_2(NCS)]$ (**2**), $[Ni^{II}_2(L^2)(O_2CMe)_2(MeOH)(H_2O)][ClO_4]$ (**3**), and $[Ni^{II}_2(L^2)(O_2CMe)_2(MeOH)(H_2O)][BPh_4]\cdot 3MeOH\cdot H_2O$ (**4**) have been synthesized [HL^1: 2,6-bis[*N*-methyl-*N*-(2-pyridylethyl)amino]-4-methylphenol; HL^2: 2,6-bis[3-(pyridin-2-yl)pyrazol-1-ylmethyl]-4-methylphenol]. Complexes **1**, **3**, and **4** are new while complex **2** was reported previously by Fenton and co-workers (the structure of **2** was presented but no physicochemical properties of this complex were reported; in this work such studies have been completed). X-ray crystallographic analyses of **1** and **4** reveal that each nickel(II) center is six-coordinate, terminally coordinated by two nitrogen donors [(pyridin-2-yl)ethylamine unit in **1** and 3-(pyridin-2-yl)pyrazole moiety in **4**], and bridged by an endogenous phenolate ion. Each of the acetate ions in **1** adopts a η^2-coordination mode (chelating) whereas in **4** each is coordinated in a $\mu-\eta^1:\eta^1$ *syn-syn* bridging mode. In **1** each Ni^{II} center has water coordination whereas in **4** one Ni^{II} center has a methanol and the other has water coordination. The X-ray structure of **3** could not be determined. The physicochemical properties (electronic spectroscopy and cyclic voltammetry) of the cation of **3** are identical to that of **4**. Magnetic susceptibility measurements have revealed the occurrence of ferromagnetic coupling of spins of the nickel(II) centers in **2** [$J = +9.80\ cm^{-1}$]. The nickel(II) centers in **1** and **3** are antiferromagnetically coupled, but to different extents [$J = -48.4\ cm^{-1}$ (**1**); $J = -1.24\ cm^{-1}$ (**3**)]. The magnetic properties are correlated with the nature of bridges between the nickel(II) ions. The two coordinated aqua ligands in **1** and the aqua and methanol ligands in **3** have enabled these dinuclear nickel(II) complexes to function as catalysts in the hydrolysis of 2-hydroxypropyl-*p*-nitrophenylphosphate (HPNP). Complex **1** is more effective in the conversion of substrate to product (*p*-nitrophenolate ion) than **3**, under identical experimental conditions. Pseudo first-order kinetic treatment has been done for complexes **1** and **3**. Temperature-dependent measurements were done to evaluate kinetic/thermodynamic parameters for the hydrolysis/transesterification reaction of HPNP and to propose a mechanistic pathway. The activation parameters are $\Delta H^{\ddagger} = 64\ kJ\ mol^{-1}$, $\Delta S^{\ddagger} = -104\ J\ mol^{-1}\ K^{-1}$ for **1** and $\Delta H^{\ddagger} = 68\ kJ\ mol^{-1}$, $\Delta S^{\ddagger} = -109\ J\ mol^{-1}\ K^{-1}$ for **3**. A mechanism consistent with the kinetic data is presented.

Introduction

Bimetallic cores exist at active sites of many enzymes and play an essential role in biological systems. The present work derives impetus from the active sites of metallohydrolases.[1,2] Model studies using simple binuclear metal complexes remain to be increasingly important to understand the biological significance of such bimetallic cores.[3] As a continuation of our activity on bioinspired coordination chemistry with phenoxo-/hydroxo-bridged dicopper(II) complexes (aromatic ring hydroxylation[4] and catechol oxidation[5] of relevance to tyrosinase and catechol oxidase, respectively), we wished to synthesize phenoxo-bridged dinickel(II) complexes with labile sites to investigate their potential as

*To whom correspondence should be addressed. E-mail: rnm@iitk.ac.in. Phone: +91-512-2597437. Fax: +91-512-2597436.

(1) (a) Sträter, N.; Lipscomb, W. N.; Klabunde, T.; Krebs, B. *Angew. Chem., Int. Ed. Engl.* **1996**, *35*, 2024–2055. (b) Dismukes, G. C. *Chem. Rev.* **1996**, *96*, 2909–2926. (c) Wilcox, D. E. *Chem. Rev.* **1996**, *96*, 2435–2458. (c) Belle, C.; Pierre, J.-L. *Eur. J. Inorg. Chem.* **2003**, 4137–4146. (d) Weston, J. *Chem. Rev.* **2005**, *105*, 2151–2174.

(2) (a) Halcrow, M. A.; Christou, G. *Chem. Rev.* **1994**, *94*, 2421–2481. (b) Lipscomb, W. N.; Sträter, N. *Chem. Rev.* **1996**, *96*, 2375–2433. (c) Perkin, G. *Chem. Rev.* **2004**, *104*, 699–767.

(3) Mitić, N.; Smith, S. J.; Neves, A.; Guddat, L. W.; Gahan, L. R.; Schenk, G. *Chem. Rev.* **2006**, *106*, 3338–3363.

(4) (a) Ghosh, D.; Mukherjee, R. *Inorg. Chem.* **1998**, *37*, 6597–6605. (b) Mandal, S.; Mukherjee, R. *Inorg. Chim. Acta* **2006**, *359*, 4019–4026. (c) De, A.; Mandal, S.; Mukherjee, R. *J. Inorg. Biochem.* **2008**, *102*, 1170–1189 and references therein.

(5) Mukherjee, J.; Mukherjee, R. *Inorg. Chim. Acta* **2002**, *337*, 429–438.

Published on Web 07/17/2009

catalysts toward hydrolysis of organic phosphate esters.[6] As a first step toward this endeavor we have synthesized three new dinickel(II) complexes $[Ni^{II}_2(L^1)(O_2CMe)_2(H_2O)_2][PF_6]\cdot MeOH\cdot 3H_2O$ (**1**), $[Ni^{II}_2(L^2)(O_2CMe)_2(MeOH)(H_2O)][ClO_4]$ (**3**), and $[Ni^{II}_2(L^2)(O_2CMe)_2(MeOH)(H_2O)][BPh_4]\cdot 3MeOH\cdot H_2O$ (**4**) derived from non-Schiff base phenol-based end-off compartmental dinucleating ligands, 2,6-bis[*N*-methyl-*N*-(2-pyridylethyl)amino]-4-methylphenol (HL^1) and 2,6-bis[3-(pyridin-2-yl)pyrazol-1-ylmethyl]-4-methylphenol (HL^2), with capability of terminal bidentate coordination. The choices of HL^1 and HL^2 are based on the following considerations. Reduction of the denticity of an endogenous phenolate bridging dinucleating ligand from more common tridentate to bidentate terminal coordination would provide an opportunity for coordination by solvent and/or suitable bridging ligands (such as acetate group) to complete six-coordination of nickel(II) centers. The crystal structure analyses of **1** and **4** have confirmed our prediction. The structural analyses of **1** and **4** allow us to compare the metric parameters due to differing coordination modes of acetate bridges present in these two phenoxo-bridged dinickel(II) complexes. In spite of our sincere attempts we failed to grow single-crystals of **3**. On the basis of identical physicochemical properties of complexes **3** and **4** it is logical to assume that the structure of the complex cation of **3** is identical to that of **4**. Magneto-structural studies on **1**, reported complex $[Ni^{II}_2(L^1)(O_2CMe)_2(NCS)]$ (**2**),[7] and **3** reveal a systematic trend: **1** [antiferromagnetic: $J = -48.4\ cm^{-1}$], **2** [weak ferromagnetic: $J = +9.80\ cm^{-1}$], and **3** [very weak antiferromagnetic: $J = -1.24\ cm^{-1}$]. The complexes **1** and **3** have two labile sites for substrate binding and to provide an H_2O/OH^- as the nucleophile, and hence are ideal candidates to explore their potential to catalyze the hydrolysis of an organophosphate ester. From this perspective, reactivity and kinetic studies of **1** and **3** toward catalysis of hydrolysis/transesterification of 2-hydroxypropyl-*p*-nitrophenylphosphate (HPNP), under optimal pH conditions, have been made. It has been revealed that **1** exhibits a significantly faster rate of hydrolysis than **3**. A mechanism consistent with the kinetic data is presented. The relevance of the complexes to mimic hydrolytic enzymes is finally discussed.

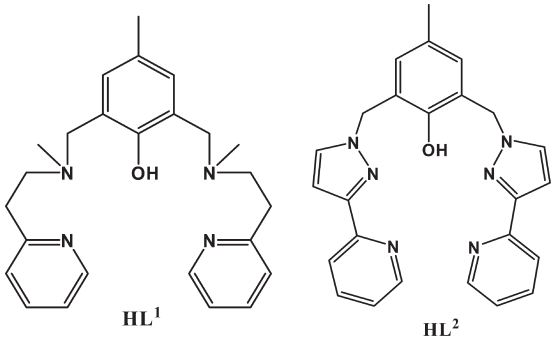

Experimental Section

Reagents and Materials. All chemicals were obtained from commercial sources and used as received. The buffers *N*-(2-hydroxyethyl)piperazine-*N*′-(2-ethanesulfonic acid) (HEPES) and [2-(*N*-cyclohexylamino)ethanesulfonic acid] (CHES) were obtained from commercial sources. Solvents were dried as reported previously.[4,5] 4-(Benzyloxy)-3,5-bis(chloromethyl)-toluene[8] and 3-(pyridin-2-yl)pyrazole[9] were prepared according to previously published methods. Tetra-*n*-butylammonium perchlorate (TBAP) was prepared as before.[4,5] The barium salt of 2-hydroxypropyl-*p*-nitrophenylphosphate (HPNP) was prepared following a literature procedure.[10]

Syntheses of Ligands. 2,6-Bis[*N*-methyl-*N*-(2-pyridylethyl)-amino]-4-methylphenol, (HL^1). It was synthesized from 2, 6-bis(chloromethyl)-4-methylphenol and (2-pyridylethyl)methylamine as described previously.[4a,11]

2,6-Bis[3-(pyridin-2-yl)pyrazol-1-ylmethyl]-4-methylphenol, (HL^2). The synthetic strategy comprises the following two steps.

4-(Benzyloxy)-3,5-bis{(3-(pyridin-2-yl)pyrazol-1-yl)methyl}-toluene. Sodium hydride (1.800 g, 0.075 mol) was suspended in *N*, *N*-dimethylformamide (DMF) (50 mL). To it was added 3-(pyridin-2-yl)pyrazole (4.350 g, 0.030 mol), under a dry dinitrogen atmosphere. The mixture was then stirred for 1 h. To this was added a solution of 4-(benzyloxy)-3,5-bis(chloromethyl)toluene (4.300 g, 0.015 mol) in DMF (25 mL) dropwise. The resulting mixture was magnetically stirred for 4 days at 298 K. Addition of water (15 mL) followed by solvent evaporation under reduced pressure afforded a slurry, to which was added an aqueous 10% NaOH solution (25 mL). The protected ligand was extracted with CH_2Cl_2 (40 mL), and the organic layer was washed with water, followed by drying over anhydrous Na_2SO_4. Solvent removal to one-third of its initial volume under reduced pressure afforded a brown oil, to which *n*-hexane (15 mL) was added to give a brownish white product (5 g, 65%).^{1}H NMR (80 MHz, $CDCl_3$): δ 8.75 (2H, *d*, pyridine H^6), 8.06 (2H, *d*, pyrazole H^5), 7.94−7.31 (13H, *m*, phenol ring protons, benzene ring protons, and pyridine H^{3-5}), 6.96 (2H, *d*, pyrazole H^4), 5.53 (4H, *s*, $-CH_2N_3C_8H_6$), 4.97 (2H, *s*, $-OCH_2Ph$), 2.22 (3H, *s*, $-CH_3$).

2,6-Bis[3-(pyridin-2-yl)pyrazol-1-ylmethyl]-4-methylphenol (HL^2). 4-(Benzyloxy)-3,5-bis{(3-(pyridin-2-yl)pyrazol-1-yl)methyl}toluene (5 g, 10.03 mmol) was refluxed with concentrated HBr (40 mL) and water (56 mL) for 10 h. The reaction mixture was then cooled to room temperature and neutralized to pH 7 with aqueous NaOH solution (10 M). The expected ligand HL^2 was then extracted with CH_2Cl_2 (40 mL), and the organic layer dried over anhydrous Na_2SO_4. The organic extract was then concentrated to one-fifth of its initial volume, and addition of *n*-hexane (∼20 mL) resulted in the precipitation of a white solid. It was filtered, washed with *n*-hexane, and air-dried (2 g, 48%). ^{1}H NMR (80 MHz, $CDCl_3$): δ 8.63 (2H, *d*, pyridine H^6), 7.89 (2H, *d*, pyrazole H^5), 7.72−6.97 (8H, *m*, phenol ring protons and pyridine H^{3-5}), 6.88 (2H, *d*, pyrazole H^4), 5.34 (4H, *s*, $-CH_2N_3C_8H_6$), 2.16 (3H, *s*, $-CH_3$); ESI−MS: 423.1931 (100%).

Syntheses of Complexes. $[Ni^{II}_2(L^1)(O_2CMe)_2(H_2O)_2][PF_6]\cdot MeOH\cdot 3H_2O$ (1). $Ni(O_2CMe)_2\cdot 4H_2O$ (0.370 g, 1.485 mmol) was added to a solution of HL^1 (0.300 g, 0.743 mmol) in MeOH (10 mL). Initially the reaction mixture was slightly warmed and finally it was refluxed for 2 h. After cooling to room temperature (298 K), an aqueous solution (5 mL) of KPF_6 (0.137 g, 0.743 mmol) was then added, stirred for 30 min, and filtered to remove any solid

(6) (a) Chin, J. *Curr. Opin. Chem. Biol.* **1997**, *1*, 514–521. (b) Hegg, E. L.; Burstyn, J. N. *Coord. Chem. Rev.* **1998**, *173*, 133–165. (c) Krämer, R. *Coord. Chem. Rev.* **1999**, *182*, 243–261. (d) Williams, N. H.; Takasaki, B.; Wall, M.; Chin, J. *Acc. Chem. Res.* **1999**, *32*, 485–493. (e) Morrow, J. R.; Iranzo, O. *Curr. Opin. Chem. Biol.* **2004**, *8*, 192–200. (f) Meyer, F. *Eur. J. Inorg. Chem.* **2006**, 3789–3800. (f) Jarenmark, M.; Carlsson, H.; Nordlander, E. *C. R. Chim.* **2007**, *10*, 433–462. (g) Mancin, F.; Tecilla, P. *New J. Chem.* **2007**, *31*, 800–817.

(7) Adams, H.; Fenton, D. E.; McHugh, P. E. *Inorg. Chem. Commun.* **2004**, *7*, 140–145.

(8) Gupta, R.; Mukherjee, S.; Mukherjee, R. *J. Chem. Soc., Dalton Trans.* **1999**, 4025–4030.

(9) Amoroso, A. J.; Thompson, A. M. C.; Jeffery, J. C.; Jones, P. L.; McCleverty, J. A.; Ward, M. D. *J. Chem. Soc., Chem. Commun.* **1994**, 2751–2752.

(10) Brown, D. M.; Usher, D. A. *J. Chem. Soc.* **1965**, 6558–6564.

(11) Karlin, K. D.; Farooq, A.; Gultneh, Y.; Hayes, J. C.; Zubieta, J. *Inorg. Chim. Acta* **1988**, *153*, 73–74.

particles. Subsequent slow evaporation of the aqueous-methanolic solution resulted in the formation of green crystals, which were filtered, and washed with cold water. Recrystallization was achieved by slow evaporation of a methanolic solution of the complex at room temperature. Single-crystals thus obtained were found to be suitable for X-ray structural studies. Yield: 0.290 g, 43%. Anal. Calcd (%) for $C_{30}H_{51}F_6N_4Ni_2O_{11}P$: C, 39.77; H, 5.67; N, 6.18. Found: C, 39.73; H, 5.35; N, 6.39. IR (KBr, cm^{-1}, selected absorption bands): 3397 (ν(OH) of water); 1607, 1576 ($\nu_{asym}(O_2CMe)$); 1475, 1448, 1423 ($\nu_{sym}(O_2CMe)$); 845 ($\nu(PF_6^-)$). Conductivity (MeOH, 10^{-3} M solution at 298 K): $\Lambda_M = 100\ \Omega^{-1}\ cm^2\ mol^{-1}$ (expected range[12] for 1:1 electrolyte: 80−115 $\Omega^{-1}\ cm^2\ mol^{-1}$). Electronic spectrum [$\lambda_{max}$, nm ($\varepsilon$, $M^{-1}\ cm^{-1}$)]: (in MeOH) 298 (4650), 375 (sh) (90), 633 (20), 770 (sh) (5), 1015 (10).

$[Ni^{II}_2(L^1)(O_2CMe)_2(NCS)]$ (2). The synthesis of this reported complex[7] was achieved in an identical procedure that was followed for the synthesis of **1**, using $Ni(O_2CMe)_2\cdot 4H_2O$ (0.370 g, 1.485 mmol), HL^1 (0.300 g, 0.743 mmol), and sodium thiocyanate (0.120 g, 1.485 mmol). Yield: 0.285 g, 55%. Anal. Calcd (%) for $C_{30}H_{37}N_5Ni_2O_5S$: C, 51.69; H, 5.35; N, 10.05. Found: C, 52.13; H, 5.35; N, 10.03. IR (KBr, cm^{-1}, selected absorption bands): 2093 ($\nu(NCS^-)$); 1578 ($\nu_{asym}(O_2CMe)$); 1480, 1418 ($\nu_{sym}(O_2CMe)$). Conductivity (MeOH, 10^{-3} M solution at 298 K): $\Lambda_M = 12\ \Omega^{-1}\ cm^2\ mol^{-1}$. Electronic spectrum [$\lambda_{max}$, nm ($\varepsilon$, $M^{-1}\ cm^{-1}$)]: (in MeOH) 298 (4200), 375 (sh) (110), 633 (20), 770 (sh) (8), 1020 (20).

$[Ni^{II}_2(L^2)(O_2CMe)_2(MeOH)(H_2O)][ClO_4]$ (3). A mixture of HL^2 (0.300 g, 0.712 mmol), $Ni(O_2CMe)_2\cdot 4H_2O$ (0.355 g, 1.424 mmol), and Et_3N (0.072 g, 0.712 mmol) in MeOH (15 mL) was refluxed for 2 h. After cooling to room temperature (298 K), solid $NaClO_4\cdot H_2O$ (0.100 g, 0.712 mmol) was then added, stirred for 30 min, and filtered to remove any solid particles. Subsequent slow evaporation of the filtrate resulted in the formation of a green microcrystalline solid. It was filtered, washed with cold water, and dried in vacuo. Yield: 0.260 g, 45%. Anal. Calcd (%) for $C_{30}H_{33}ClN_6Ni_2O_{11}$: C, 44.68; H, 4.12; N, 10.42. Found: C, 44.92; H, 4.15; N, 10.46. IR (KBr, cm^{-1}, selected absorption bands): 3431 (ν(OH) of H_2O/MeOH); 1609, 1570 ($\nu_{sym}(O_2CMe)$); 1439, 1420 ($\nu_{asym}(O_2CMe)$); 1088, 627 ($\nu(ClO_4^-)$). Conductivity (MeOH, 10^{-3} M solution at 298 K): $\Lambda_M = 95\ \Omega^{-1}\ cm^2\ mol^{-1}$. Electronic spectrum [$\lambda_{max}$, nm ($\varepsilon$, $M^{-1}\ cm^{-1}$)]: (in MeOH) 240 (42 930), 289 (33 600), 636 (42), 750 (sh) (30), 980 (35).

$[Ni^{II}_2(L^2)(O_2CMe)_2(MeOH)(H_2O)][BPh_4]\cdot 3MeOH\cdot H_2O$ (4). This compound was synthesized only to get single-crystals suitable for X-ray structure determination. It was prepared by following a procedure as described for **3**; however, using $NaBPh_4$ instead of $NaClO_4\cdot H_2O$. Anal. Calcd (%) for $C_{57}H_{67}BN_6Ni_2O_{11}$: C, 60.03; H, 5.92; N, 7.37. Found: C, 60.17; H, 5.75; N, 7.35. IR (KBr, cm^{-1}, selected absorption bands): 3420 (ν(OH) of H_2O/MeOH); 1610, 1571 ($\nu_{asym}(O_2CMe)$); 1434, 1417 ($\nu_{sym}(O_2CMe)$); 737, 705 ($\nu(BPh_4^-)$). Conductivity (MeOH, 10^{-3} M solution at 298 K): $\Lambda_M = 90\ \Omega^{-1}\ cm^2\ mol^{-1}$. Electronic spectrum [$\lambda_{max}$, nm ($\varepsilon$, $M^{-1}\ cm^{-1}$)]: (in MeOH) 240 (43 200), 289 (30 000), 636 (40), 750 (sh) (25), 980 (30).

Physical Measurements. Elemental analyses were obtained using a Thermo Quest EA 1110 CHNS-O, Italy. Conductivity measurements were done with an Elico type CM-82T conductivity bridge (Hyderabad, India). Spectroscopic measurements were made using the following instruments: IR (KBr, 4000−600 cm^{-1}), Bruker Vector 22; electronic, Agilent 8453 diode-array spectrophotometer; ESI−MS: Waters-HAB213 spectrometer. ^1H NMR spectra ($CDCl_3$ solution) were obtained on a Bruker WP-80 (80 MHz) spectrometer. Chemical shifts are reported in ppm referenced to TMS. ^{31}P NMR spectra (MeOH−H_2O solution, 33%) were recorded on a JEOL JNM LA 500 (500 MHz) spectrometer. Chemical shifts are reported with respect to 85% H_3PO_4 as the external standard.

Magnetic susceptibility measurements in the temperature range 2−300 K were carried out on polycrystalline samples of **1**, **2**, and **3** with a Quantum Design (MPMSXL-5) SQUID magnetic susceptometer at València, Spain. Solution-state magnetic susceptibilities were obtained by the NMR technique of Evans[13] in CH_2Cl_2 with a JEOL JNM LA 400 (400 MHz) spectrometer and made use of the paramagnetic shift of the methylene protons of CH_2Cl_2 as the measured NMR parameter.

Cyclic voltammetric (CV) measurements were performed at 298 K by using a CH Instruments Electrochemical Analyzer/Workstation Model 600B Series. The cell contained a Beckman (M-39273) platinum-inlay working electrode, a platinum wire auxiliary electrode, and a saturated calomel electrode (SCE) as reference electrode. Details of the cell configuration are as described before.[14] The solutions were ~1.0 mM in complex and 0.1 M in supporting electrolyte TBAP.

Crystal Structure Determination. X-ray data of complexes **1** and **4** were collected on a Bruker SMART APEX CCD diffractometer at 100(2) K, with graphite-monochromated Mo−Kα ($\lambda = 0.71073$ Å) radiation. For data reduction the "Bruker Saint Plus" program was used. Data were corrected for Lorentz and polarization effects; empirical absorption correction (SADABS) was applied. Structures were solved by SIR-97 and refined by full-matrix least-squares methods based on F^2 using SHELXL-97, incorporated in the WinGX 1.64 crystallographic collective package.[15] For **1**, some disorder was encountered with oxygen atom of one water molecule, which was refined with a site occupation factor of 55/45. For **4**, some disorder was encountered with carbon atoms of two methanol molecules and oxygen of the water molecule, which were refined with a site occupation factor of 70/30 and 80/20, respectively. For **1** and **4** all non-hydrogen atoms [in the case of **4** excluding disordered carbon groups of a methanol molecule (C3SA and C3SB)] were refined anisotropically. For **4** the disordered oxygen atoms of water molecule OWA and OWB were refined with equal thermal parameters, using EADP command. One methanolic C−O distance (C2SB−O2S) was restrained to obtain a reasonable bond distance. For **4** two residual peaks 1.03 e $Å^{-3}$ and 1.00 e $Å^{-3}$ could not be assigned; this may be due to the poor quality of crystal chosen for data collection. The crystal was not of good quality, but the data collection was still done for such a crystal, as it was the best we could have. Except for four hydrogen atoms in **1** and three hydrogen atoms in **4** (positions were located from the difference Fourier map), the positions of the hydrogen atoms were calculated assuming ideal geometries. We could not locate the hydrogen atoms of water molecules O1W, O2W, and O3W in **1** and OW in **4**. We could not assign the methanol O−H hydrogen atoms of two disordered methanol molecules in **4**. Pertinent crystallographic parameters are summarized in Table 1.

Potentiometric Measurements. Potentiometric titrations were carried out at 25 °C using Metrohm 794 Basic Titrino connected with a Metrohm AG 9101 Herisau pH glass-electrode and a ground-joint diaphragm. Before experiment, the standardization was done with aqueous buffer solutions at pH 4.00 and 7.00. Solutions were made up with aqueous methanol (33%, v/v), and the ionic strength was adjusted to 0.1 M by adding appropriate amounts of $NaNO_3$. To compensate for the expected methanol−water liquid junction potential, a correction of 0.051 pH

(12) Geary, W. J. *Coord. Chem. Rev.* **1971**, *7*, 81–122.

(13) Evans, D. F. *J. Chem. Soc.* **1959**, 2003–2005.

(14) Gupta, N.; Mukerjee, S.; Mahapatra, S.; Ray, M.; Mukherjee, R. *Inorg. Chem.* **1992**, *31*, 139.

(15) Farrugia, L. J. *WinGX version 1.64, An Integrated Systems of Windows Programs for the Solution, Refinement and Analysis of Single-Crystal X-ray Diffraction Data*; Department of Chemistry, University of Glasgow: Glasgow, U.K., 2003.

Table 1. Data Collection and Structure Refinement Parameters for $[Ni^{II}_2(L^1)(O_2CMe)_2(H_2O)_2][PF_6]\cdot MeOH\cdot 3H_2O$ (**1**) and $[Ni^{II}_2(L^2)(O_2CMe)_2(MeOH)(H_2O)][BPh_4]\cdot 3MeOH\cdot H_2O$ (**4**)

	1	**4**
chemical formula	$C_{30}H_{51}F_6N_4Ni_2O_{11}P$	$C_{57}H_{67}BN_6Ni_2O_{11}$
formula weight	906.09	1140.37
crystal color, habit	green, cube	green, cube
temperature (K)	100(2)	100(2)
λ (Å)	Mo−K_α (0.71073)	Mo−K_α (0.71073)
crystal system	monoclinic	triclinic
crystal size/(mm × mm × mm)	0.2 × 0.2 × 0.2	0.2 × 0.2 × 0.2
space group	$P2_1/n$ (No.14)	$P\bar{1}$ (No.2)
a (Å)	12.823(5)	13.177(5)
b (Å)	22.853(5)	15.239(5)
c (Å)	13.453(5)	16.124(5)
α (deg)	90.0	107.596(5)
β (deg)	95.938(5)	104.976(5)
γ (deg)	90.0	102.328(5)
V (Å^3)	3921(2)	2828.0(17)
Z	4	2
D_c (g cm^{-3})	1.525	1.335
μ (mm^{-1})	1.088	0.730
reflections mesured	25948	19140
unique reflections [R_{int}]	9684 (R_{int} = 0.0524)	13523 (R_{int} = 0.0388)
number of reflections used [$I > 2\sigma(I)$]	6919	8844
number of parameters	514	723
final R indices	R_1 = 0.0622[a] wR_2 = 0.1404[b]	R_1 = 0.0844[a] wR_2 = 0.1895[b]
R indices (all data)	R_1 = 0.0976[a] wR_2 = 0.1916[b]	R_1 = 0.1336[a] wR_2 = 0.2382[b]
Goodness-of-fit on F^2	1.135	1.108

[a] $R_1 = \sum||F_o| - |F_c||/\sum|F_o|$. [b] $wR_2 = \{\sum w(F_o^2 - F_c^2)^2/\sum w(F_o^2)^2\}^{1/2}$.

units were subtracted from the measured pH readings.[16] Computations were carried out with the HYPERQUAD 2000 program, and species distributions were calculated using the program HySS.[17]

To determine the pKa values of the coordinated water molecules in $[Ni^{II}_2(L^1)(O_2CMe)_2(H_2O)_2][PF_6]\cdot MeOH\cdot 3H_2O$ (**1**) and $[Ni^{II}_2(L^2)(O_2CMe)_2(MeOH)(H_2O)][ClO_4]$ (**3**), a typical pH-metric titration was done as follows: A 33% MeOH−H_2O 1 mM solutions of complexes **1** and **3** were titrated with a 0.01 N NaOH solution. The ionic-strength of the medium was maintained at I = 0.1 M $NaNO_3$.

Kinetic Experiments. Phosphatase-like activities of complexes **1** and **3** were determined through the hydrolysis reaction of the model substrate 2-hydroxypropyl-*p*-nitrophenylphosphate (HPNP), under pseudo first-order conditions (excess complex concentration). To determine the activity toward phosphate ester cleavage, the increase of the concentration of *p*-nitrophenolate was followed by UV−vis spectroscopy at 400 nm (ε = 18 500 M^{-1} cm^{-1}),[18] using an Agilent 8453 diode-array spectrophotometer, equipped with a 89090A temperature-controller. The observed pseudo first-order rate constant (k_{obs}) values were obtained by the equation: $d([PNP]_{total})/dt = k_{obs}[HPNP]_0$. With respect to a pH-dependent equilibrium between *p*-nitrophenol (PNPh) and *p*-nitrophenolate (PNPate) the increase of the concentration of the reaction product can be calculated (pH = pK_S + log-[PNPate]/[PNPh]) by using the pK_S value of 7.15.[18] The kinetic studies were performed in MeOH−H_2O (33%, v/v). The solution was buffered using HEPES or CHES (20 mM) and the ionic strength was maintained at I = 0.1 M $NaNO_3$. Studies regarding the effect of pH on the hydrolysis reaction were performed in the pH range 7.00−10.00 (HEPES pH 7.00−8.00; CHES pH 8.50−10.00), under a 10-fold excess of the complex, at 30 °C. Experiments to determine the dependence of the reaction rate on the complex concentration were carried out at 30 °C, pH 8.50, [HPNP] = 5×10^{-5} M, [complex] = 25 × 10^{-5} to 125 × 10^{-5} M, for both complexes. The effect of temperature on the reaction rate was investigated in the range 30−45 °C at pH 8.50 and a 10-fold excess of complex (50 × 10^{-5} M) relative to substrate (5 × 10^{-5} M) was maintained. The influence of acetate on the reaction rate was evaluated, at pH 8.50, 30 °C, and a 10-fold substrate excess (4.62×10^{-4} M) relative to the complex (4.62×10^{-5} M). In all the cases the complex solution was mixed with buffer solution in a thermostatted UV cell and was left for 0.5 h for temperature equilibration prior to the addition of substrate. All kinetic experiments were run twice and average values were taken. In all of these experiments, the spontaneous hydrolysis was corrected by direct difference between two identical parallel reactions, but without addition of catalyst in one of them. Michaelis−Menten kinetic study has also been invoked (Supporting Information).

Monitoring of Hydrolysis Products of HPNP by ^{31}P NMR. The hydrolysis of 2.30 × 10^{-3} M solution of HPNP with 4.62 × 10^{-5} M of the catalyst (complex **1**) was investigated by ^{31}P NMR spectroscopy at 30 °C in 33% MeOH−H_2O buffered with CHES (20 mM) at pH 8.50, I = 0.1 M $NaNO_3$. The reaction was followed by monitoring the appearance of the signal at 17.98 ppm[19] corresponding to the cyclic phosphodiester formed after the release of *p*-nitrophenolate anion (the chemical shift value is with respect to 85% H_3PO_4 as the external standard).

(16) Bates, R. G.; Paabo, M.; Robinson, R. A. *J. Phys. Chem.* **1963**, *67*, 1833–1838.

(17) (a) Gans, P.; Sabatini, A.; Vacca, A. *Talanta* **1996**, *43*, 1739–1753. (b) Alderighi, A.; Gans, P.; Ienco, A.; Peters, D.; Sabatini, A.; Vacca, A. *Coord. Chem. Rev.* **1999**, *184*, 311–318.

(18) Jarenmark, M.; Kappen, S.; Haukka, M.; Nordlander, E. *Dalton Trans.* **2008**, 993–996.

(19) Selmeczi, K.; Michel, C.; Milet, A.; Gautier-Luneau, I.; Philouze, C.; Pierre, J- L.; Schnieders, D.; Rompel, A.; Belle, C. *Chem.—Eur. J.* **2007**, *13*, 9093–9106.

Results and Discussion

Complexes. Phenol-based ligands, possessing chelating arms attached to the 2- and 6-positions of the phenolic ring, have often been used for modeling bimetallic biosites.[20] The synthesis of the ligand HL^1 is reported in the literature.[4a,11] The new ligand HL^2 has been synthesized following the methodology followed before from this laboratory for the synthesis of a similar ligand 2,6-bis-(pyrazol-1-yl)methyl)-4-methylphenol.[8] The new ligand HL^2 was characterized by ^{1}H NMR and ESI−MS spectroscopy. The reaction of the ligand HL^1 with $Ni(O_2CMe)_2\cdot 4H_2O$ in MeOH followed by addition of aqueous solution of KPF_6 afforded isolation of the compound $[Ni^{II}_2(L^1)(O_2CMe)_2(H_2O)_2][PF_6]\cdot MeOH\cdot 3H_2O$ (**1**). A similar reaction using NaNCS instead of KPF_6 afforded isolation of the microcrystalline solid $[Ni^{II}_2(L^1)(O_2CMe)_2(NCS)]$ (**2**). It should be mentioned here that although the structure of compound **2** is reported in the literature, but not other properties.[7] In this investigation we report on the spectral, magnetic, and redox properties of **2**. Similarly, the reaction of ligand HL^2 with $Ni(O_2CMe)_2\cdot 4H_2O$ and Et_3N in MeOH followed by addition of $NaClO_4\cdot H_2O$ as a solid afforded isolation of the compound $[Ni^{II}_2(L^2)(O_2CMe)_2(MeOH)(H_2O)][ClO_4]$ (**3**). The complex $[Ni^{II}_2(L^2)(O_2CMe)_2(MeOH)(H_2O)][BPh_4]\cdot 3MeOH\cdot H_2O$ (**4**) was synthesized to grow single-crystals suitable for crystallographic analysis (see below).

Complex **2** is a non-electrolyte in MeOH, while **1**, **3**, and **4** have molar conductance values typical for a 1:1 electrolyte in this solvent.[12]

Spectroscopic Characterization. Complex **1** shows the characteristic IR bands of the coordinated acetate group for the antisymmetric stretching (1607 and 1576 cm^{-1}) and for the symmetric stretching (1475, 1448, and 1423 cm^{-1}) vibrations. The small separation (< 200 cm^{-1})[21] between the two vibrations suggests a bidentate chelating mode for the acetato ligand in **1**. Small separations are also observed for **2**, **3**, and **4** as each complex has acetate groups coordinated in μ_2-1,3-bridging mode. Complex **2** shows a distinct ν(CN) mode for the NCS^- group at 2093 cm^{-1}. Complexes **1**, **3**, and **4** display intense absorptions at 845 cm^{-1}, at 1088 and 627 cm^{-1}, and at 705 cm^{-1}, characteristic of the presence of PF_6^-, ClO_4^-, and BPh_4^- counteranions, respectively. A broad absorption band at ~3400 cm^{-1} due to ν(OH) of water/methanol was observed for complexes **1**, **3**, and **4**.

The electronic spectra of **1**−**4** in MeOH suggest that each complex has grossly octahedral environment for the two

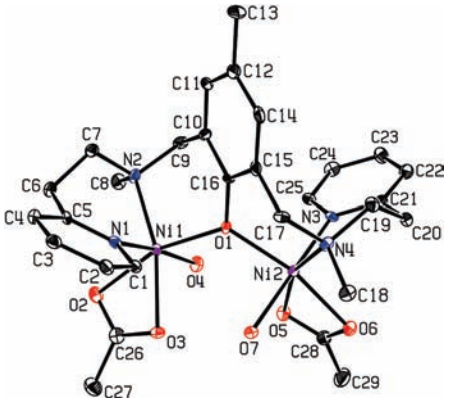

Figure 1. ORTEP view (30% probability) of the metal coordination environment in the crystal of $[Ni^{II}_2(L^1)(O_2CMe)_2(H_2O)_2][PF_6]\cdot MeOH\cdot 3H_2O$ (**1**). Hydrogen atoms are omitted for clarity.

Ni^{II} ions.[22−26] The spectra are displayed in the Supporting Information, Figures S1−S4. Two broad d-d transitions at ~635 nm and ~1000 nm (the ε values of the absorption bands range from 10 to 42 M^{-1} cm^{-1}) are observed, which can be assigned to the $^3A_{2g} \rightarrow {}^3T_{1g}(F)$ and $^3T_{2g}(F)$ transitions, respectively. For these complexes a shoulder is clearly observable in the region 750−770 nm (the ε values of the shoulder range from 5 to 30 M^{-1} cm^{-1}), which is ascribed to the spin-forbidden transition $^3A_{2g} \rightarrow {}^1E_{1g}$. For **1** and **2**, another spin-allowed d-d transition is observed as a shoulder at 375 nm ($\varepsilon = 90$ M^{-1} cm^{-1} for **1** and 110 M^{-1} cm^{-1} for **2**) due to the $^3A_{2g} \rightarrow {}^3T_{1g}(P)$ transition.

Description of Structures. (a). $[Ni^{II}_2(L^1)(O_2CMe)_2(H_2O)_2][PF_6]\cdot MeOH\cdot 3H_2O$ (1). A perspective view of the cationic part of **1** is shown in Figure 1. Selected interatomic distances and angles are listed in Table 2. Structural analysis reveals a dinuclear six-coordinate nickel(II) complex bridged by the phenolate ion of the deprotonated dinucleating ligand (HL^1) with a Ni···Ni separation of 3.6445(15) Å. Each Ni^{II} ion is terminally coordinated by one pyridine (N1/N3) and one tertiary aliphatic amine (N2/N4) donor atoms from the (pyridin-2-yl)alkylamine unit of the ligand, a bidentate acetate ion (O2 and O3; O5 and O6), and a water molecule (O4/O7). Chelation from the terminal (pyridin-2-yl)ethylamine provides six-membered chelate rings at each Ni^{II} ion, as observed before.[25,27] The Ni^{II} centers assume pseudo-octahedral N_2O_4 coordination sphere (Table 2). For endogenous phenoxo-bridged dinickel(II) complexes, coordination of a water molecule at each metal center is notable.[28]

(b). $[Ni^{II}_2(L^1)(O_2CMe)_2(NCS)]$ (2). Figure 2 depicts a schematic representation of the reported[7] crystal structure of **2**. Notably, the monodentate carboxylate bridge causes distortion of octahedral coordination environment of Ni^{II} ions.

(20) Ōkawa, H.; Furutachi, H.; Fenton, D. E. *Coord. Chem. Rev.* **1998**, *174*, 51–75.
(21) Deacon, G. B.; Phillips, R. J. *Coord. Chem. Rev.* **1980**, *33*, 227–250.
(22) Volkmer, D.; Hommerich, B.; Griesar, K.; Haase, W.; Krebs, B. *Inorg. Chem.* **1996**, *35*, 3792–3803.
(23) Cotton, F. A.; Wilkinson, G. *Advanced Inorganic Chemistry*, 5th ed.; Wiley: New York, 1988.
(24) Buchanan, R. M.; Mashuta, M. S.; Oberhausen, K. J.; Richardson, J. F. *J. Am. Chem. Soc.* **1989**, *111*, 4497–4498.
(25) (a) Gultneh, Y.; Raza Khan, A.; Ahvazi, B.; Butcher, R. J. *Polyhedron* **1998**, *17*, 1751–1760. (b) Greatti, A.; Scarpellini, M.; Peralta, R. A.; Casellato, A.; Bortoluzzi, A. J.; Xavier, F. R.; Jovito, R.; de Brito, M. A.; Szpoganicz, B.; Tomkowicz, Z.; Rams, M.; Haase, W.; Neves, A. *Inorg. Chem.* **2008**, *47*, 1107–1119 and references therein.
(26) Greatti, A.; de Brito, M. A.; Bortoluzzi, A. J.; Ceccato, A. S. *J. Mol. Struct.* **2004**, *688*, 185–190.
(27) (a) Adams, H.; Clunas, S.; Fenton, D. E.; Gregson, T. J.; McHugh, P. E.; Spey, S. E. *Inorg. Chem. Commun.* **2002**, *5*, 211–214. (b) Adams, H.; Clunas, S.; Fenton, D. E.; Spey, S. E. *J. Chem. Soc., Dalton Trans.* **2002**, 441–448. (c) Fenton, D. E. *Inorg. Chem. Commun.* **2002**, *5*, 537–547. (d) Adams, H.; Clunas, S.; Fenton, D. E.; Gregson, T. J.; McHugh, P. E.; Spey, S. E. *Inorg. Chim. Acta* **2003**, *346*, 239–247.
(28) (a) de Brito, M. A.; Bortoluzzi, A. J.; Greatti, A.; Ceccato, A. S.; Joussef, A. C.; Drechsel, S. M. *Acta Crystallogr.* **2000**, *C56*, 1188–1190. (b) Pal Chaudhuri, U.; Varghese, B.; Murthy, N. N. *Acta Crystallogr.* **2003**, *E59*, m627–m629.

Table 2. Selected Bond Lengths (Å) and Bond Angles (deg) in the Cationic Parts of $[Ni^{II}_2(L^1)(O_2CMe)_2(H_2O)_2][PF_6]\cdot MeOH\cdot 3H_2O$ (**1**) and $[Ni^{II}_2(L^2)(O_2CMe)_2(MeOH)(H_2O)][BPh_4]\cdot 3MeOH\cdot H_2O$ (**4**)

1		**4**	
Ni(1)−N(1)	2.059(4)	Ni(1)−N(1)	2.125(5)
Ni(1)−N(2)	2.086(4)	Ni(1)−N(2)	2.024(4)
Ni(1)−O(1)	2.040(3)	Ni(1)−O(1)	2.018(3)
Ni(1)−O(2)	2.135(3)	Ni(1)−O(2)	2.072(4)
Ni(1)−O(3)	2.145(3)	Ni(1)−O(4)	1.999(4)
Ni(1)−O(4)	2.089(4)	Ni(1)−O(6)	2.122(5)
Ni(2)−N(3)	2.061(4)	Ni(2)−N(5)	2.030(4)
Ni(2)−N(4)	2.090(4)	Ni(2)−N(6)	2.118(4)
Ni(2)−O(1)	2.047(3)	Ni(2)−O(1)	2.021(3)
Ni(2)−O(5)	2.155(3)	Ni(2)−O(3)	2.012(4)
Ni(2)−O(6)	2.115(3)	Ni(2)−O(5)	2.052(3)
Ni(2)−O(7)	2.075(4)	Ni(2)−O(7)	2.131(4)
Ni(1)···Ni(2)	3.6445(15)	Ni(1)···Ni(2)	3.3637(13)
N(1)−Ni(1)−N(2)	93.05(16)	N(1)−Ni(1)−N(2)	76.98(18)
N(1)−Ni(1)−O(1)	93.20(13)	N(1)−Ni(1)−O(1)	167.32(17)
N(1)−Ni(1)−O(2)	90.38(14)	N(1)−Ni(1)−O(2)	93.35(18)
N(1)−Ni(1)−O(3)	87.88(14)	N(1)−Ni(1)−O(4)	89.17(17)
N(1)−Ni(1)−O(4)	173.78(15)	N(1)−Ni(1)−O(6)	84.2(2)
N(2)−Ni(1)−O(1)	96.44(14)	N(2)−Ni(1)−O(1)	94.89(16)
N(2)−Ni(1)−O(2)	100.87(15)	N(2)−Ni(1)−O(2)	89.26(17)
N(2)−Ni(1)−O(3)	162.13(14)	N(2)−Ni(1)−O(4)	165.94(17)
N(2)−Ni(1)−O(4)	93.16(16)	N(2)−Ni(1)−O(6)	91.30(19)
O(1)−Ni(1)−O(2)	162.10(13)	O(1)−Ni(1)−O(2)	96.29(15)
O(1)−Ni(1)−O(3)	101.32(12)	O(1)−Ni(1)−O(4)	98.34(15)
O(1)−Ni(1)−O(4)	86.38(14)	O(1)−Ni(1)−O(6)	86.35(17)
O(2)−Ni(1)−O(3)	61.27(13)	O(2)−Ni(1)−O(4)	93.98(17)
O(2)−Ni(1)−O(4)	88.17(15)	O(2)−Ni(1)−O(6)	177.25(18)
O(3)−Ni(1)−O(4)	86.12(14)	O(4)−Ni(1)−O(6)	84.84(19)
N(3)−Ni(2)−N(4)	93.48(15)	N(5)−Ni(2)−N(6)	77.11(18)
N(3)−Ni(2)−O(1)	93.69(14)	N(5)−Ni(2)−O(1)	95.74(17)
N(3)−Ni(2)−O(5)	87.45(14)	N(5)−Ni(2)−O(3)	167.89(17)
N(3)−Ni(2)−O(6)	90.90(14)	N(5)−Ni(2)−O(5)	89.47(17)
N(3)−Ni(2)−O(7)	174.14(15)	N(5)−Ni(2)−O(7)	92.37(18)
N(4)−Ni(2)−O(1)	96.12(14)	N(6)−Ni(2)−O(1)	169.53(14)
N(4)−Ni(2)−O(5)	160.88(14)	N(6)−Ni(2)−O(3)	91.00(16)
N(4)−Ni(2)−O(6)	99.27(14)	N(6)−Ni(2)−O(5)	91.64(16)
N(4)−Ni(2)−O(7)	92.29(16)	N(6)−Ni(2)−O(7)	86.24(17)
O(1)−Ni(2)−O(5)	102.88(12)	O(1)−Ni(2)−O(3)	95.73(15)
O(1)−Ni(2)−O(6)	163.63(13)	O(1)−Ni(2)−O(5)	95.97(15)
O(1)−Ni(2)−O(7)	86.73(14)	O(1)−Ni(2)−O(7)	86.42(16)
O(5)−Ni(2)−O(6)	61.62(13)	O(3)−Ni(2)−O(5)	93.19(17)
O(5)−Ni(2)−O(7)	86.76(14)	O(3)−Ni(2)−O(7)	84.48(18)
O(6)−Ni(2)−O(7)	87.14(14)	O(5)−Ni(2)−O(7)	176.82(18)
Ni(1)−O(1)−Ni(2)	126.19(16)	Ni(1)−O(1)−Ni(2)	112.78(16)

(c). $[Ni^{II}_2(L^2)(O_2CMe)_2(MeOH)(H_2O)][BPh_4]\cdot 3MeOH\cdot H_2O$ (4). A view of the cationic part of **4** is shown in Figure 3. Selected bond distances and angles are given in Table 2. The complex has a dinuclear core bridged by the deprotonated phenolic oxygen of HL^2 and two acetate groups in the syn-syn μ_2-1,3-bridging mode, providing a (μ-phenoxo)bis(μ-carboxylato)dinickel(II) core[25b,26] with a Ni···Ni separation of 3.3637(13) Å. The terminal coordination at each Ni^{II} center is achieved by pyrazole (N2/N5) and a pyridine (N1/N6). Unlike that in **1**, terminal N donors provide five-membered chelate rings at each Ni^{II} center. The sixth coordination of one nickel center is satisfied by a water molecule and for the other center by a methanol molecule (Table 2). A similar situation was encountered before.[22]

X-ray crystallographic studies on urease (catalyzes the hydrolysis of urea to form ammonia and carbon dioxide)[1c,2a,29] from different sources have revealed that the two Ni^{II} ions are bridged by the carboxylate function of a carbamylated lysine residue and a bridging water molecule or hydroxide ion (Ni···Ni distance: ~3.5−3.7 Å). Each Ni(II) ion is ligated by two histidine residues from the protein and terminally coordinated by a water molecule. One Ni(II) ion is further ligated by an aspartate residue. Consequently, one Ni^{II} ion has a distorted square pyramidal environment (N_2O_3) and the other a pseudo-octahedral environment (N_2O_4). On the basis of this information, complexes **1** and **4** could be considered as structural models for ureases.

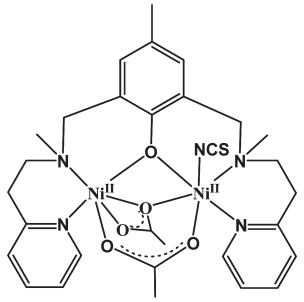

Figure 2. Schematic representation of the structure of $[Ni^{II}_2(L^1)(O_2CMe)_2(NCS)]$ (**2**). Adapted from ref 7.

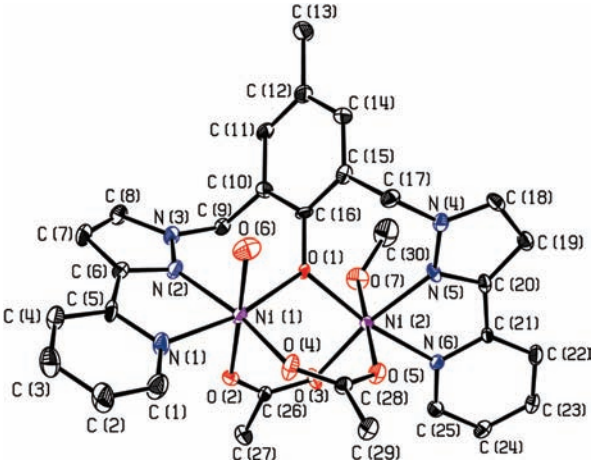

Figure 3. ORTEP view (30% probability) of the metal coordination environment in the crystal of $[Ni^{II}_2(L^2)(O_2CMe)_2(MeOH)(H_2O)][BPh_4]\cdot 3MeOH\cdot H_2O$ (**4**). Hydrogen atoms are omitted for clarity.

(d). Comparison of Metric Parameters. A closer look at the molecular structures of **1**, **2**,[7] and **4** reveal the following significant differences. (i) Both the acetato ligands present in **1** coordinate in a η^2-coordination mode (chelating). In complex **2**, one acetato ligand is coordinated in a μ_2-1,3 *syn-syn* bidentate bridging fashion whereas the other adopts a μ_2-1,1 monodentate bridging mode. In complex **4** each of the acetate ligands is coordinated in a μ_2-1,3 *syn-syn* bridging mode. (ii) While in **1** the coordination geometry is fully symmetric with donor sets $\{N_2O_4\}$, in **2** it has coordination asymmetry with donor sets $\{N_2O_4\}$ and $\{N_3O_3\}$. In **4** the coordination geometry is very close to symmetric with donor sets $\{N_2O_4\}$. (iii) The phenolate bridge is non-symmetric in **1**, **2**, and **4** but the extent of asymmetry is more in **1** and **2**. (iv) A noteworthy feature of the three structures is the

(29) (a) Karplus, P. A.; Pearson, M. A.; Hausinger, R. P. *Acc. Chem. Res.* **1997**, *30*, 330–337. (b) Lippard, S. J. *Science* **1995**, *268*, 996–997. (c) Jabri, E.; Carr, M. B.; Hausinger, R. P.; Karplus, P. A. *Science* **1995**, *268*, 998–1004.

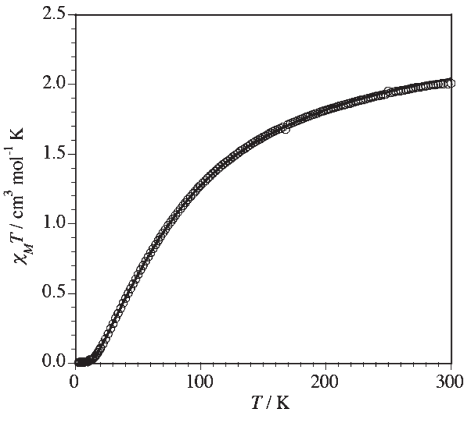

Figure 4. $\chi_M T$ vs T plot of $[Ni^{II}_2(L^1)(O_2CMe)_2(H_2O)_2][PF_6]\cdot MeOH\cdot 3H_2O$ (**1**). The solid line corresponds to the best theoretical fit (see text).

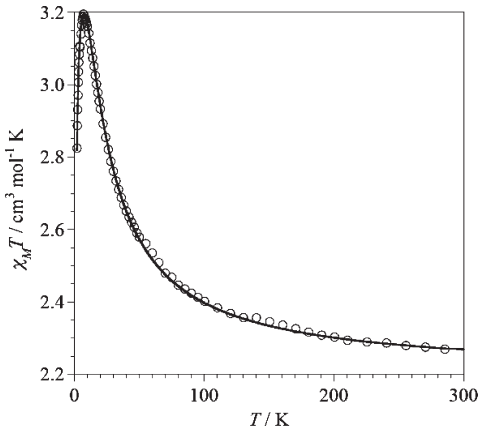

Figure 5. $\chi_M T$ vs T plot of $[Ni^{II}_2(L^1)(O_2CMe)_2(NCS)]$ (**2**). The solid line corresponds to the best theoretical fit (see text).

variation in the intramolecular Ni···Ni distances, from 3.6445(15) Å (**1**) (singly phenoxo bridge) to 3.1186(9) Å (**2**) [phenoxo and two acetate bridges (one monodentate and one bidentate bridges)] to 3.3637(13) Å (**4**) (phenoxo and two bidentate acetate bridges).

Magnetic Properties. To extract information about the nature and extent of magnetic exchange interaction between the two nickel(II) centers in three well-characterized phenoxo-bridged dinickel(II) complexes, variable-temperature (2−300 K) magnetic susceptibility measurements were carried out on powder samples of **1**−**3**. The values of $\chi_M T$ (cm^3 mol^{-1} K) at room temperature are 2.01 (**1**), 2.27 (**2**), and 2.24 (**3**) [μ_{eff}/Ni (μ_B) at 300 K: 2.84 (**1**), 3.02 (**2**), and 2.97 (**3**)]. The $\chi_M T$ values for **1** (Figure 4) and **3** (Supporting Information, Figure S5) gradually decrease with decreasing temperature, indicating the presence of an antiferromagnetic exchange interaction between the nickel(II) ions. The χ_M versus T plot for **1** (Supporting Information, Figure S6), presents a maximum at 70 K. No maximum was observed for **3** above 2 K. On the contrary, for **2** the $\chi_M T$ values gradually increase with decreasing temperature (Figure 5), attesting the presence of a ferromagnetic exchange interaction. The $\chi_M T$ versus T plot presents a maximum (3.19 cm^3 mol^{-1} K) at 7 K and then decreases until a value of 2.82 cm^3 mol^{-1} K at 2 K. The decrease of the $\chi_M T$ values at low temperatures can be due to a zero-field splitting of the $S = 2$ ground spin state and/or intermolecular antiferromagnetic exchange interactions.

The ground state of a nickel(II) ion in an octahedral environment is orbitally nondegenerate, and as such, it is possible to represent the intradimer magnetic exchange interaction (J) by two equivalent $S = 1$ ions with the isotropic Heisenberg−Dirac−van Vleck spin-exchange Hamiltonian $H = -JS_1S_2$.[30] The cryomagnetic molar magnetic susceptibility data of **1** may be expressed by eq 1, where N, β, g, k, and T have their usual meanings.

$$\chi_M = 2N\beta^2g^2/kT[\{\exp(J/kT)+5\exp(3J/kT)\}/\{1+3\exp(J/kT)+5\exp(3J/kT)\}](1-\rho)+(2N\beta^2g^2/3kT)\rho \quad (1)$$

A corrective term (ρ), the mole fraction of possible contamination of monomeric nickel(II) impurity behaving as a Curie paramagnet, has been included. Least-squares fit of the data yielded the parameters $g = 2.12$, $J = -48.4$ cm^{-1}, and $\rho = 0.004$ (0.4%). Although nickel(II) ion in axial symmetry can have a large zero-field splitting (D), the magnetic behavior of nickel(II) dimers closely follows eq 1 when a relatively strong antiferromagnetic interaction is involved ($|J| \gg |D|$).[30b] If the antiferromagnetic exchange coupling is weak or the coupling is ferromagnetic, the influence of D must be taken into account to describe the magnetic behavior at low temperatures.[30] The occurrence of a relatively large intradimer antiferromagnetic exchange coupling in **1** makes unnecessary the consideration of D, and a good fit of the experimental data to eq 1 is obtained (Figure 4).

In the cases of **2** and **3**, with intramolecular ferro- (**2**) and weak antiferromagnetic (**3**) exchange interactions, the experimental data were modeled using the Hamiltonian, $H = -J\hat{S}_1\hat{S}_2 + D(\hat{S}z_1^2 + \hat{S}z_2^2)$, with $S_1 = S_2 = 1$. To reduce the number of variables, D (zero-field splitting parameter) and g values ($g_x = g_y = g_z$) were considered to be identical for the two nickel(II) centers. Satisfactory fits were obtained with the parameters: $g = 2.10$, $|D| = 4.90$ cm^{-1}, and $J = +9.80$ cm^{-1} for **2**; $g = 2.12$, $|D| = 2.83$ cm^{-1}, and $J = -1.24$ cm^{-1} for **3**. It should be mentioned here that it is not possible to determine the sign of D from powder susceptibility measurements.[30b,c] The values of J are in reasonable agreement with the magnetic exchange interactions observed for related dinickel(II) complexes.[22,25b,31]

(30) (a) Chaudhuri, P.; Küppers, H.-J.; Wieghardt, K.; Gehring, S.; Haase, W.; Nuber, B.; Weiss, J. *J. Chem. Soc., Dalton Trans.* **1988**, 1367–1370. (b) De Munno, G.; Julve, M.; Lloret, F.; Derory, A. *J. Chem. Soc., Dalton Trans.* **1993**, 1179–1184. (c) Román, P.; Guzmán-Miralles, C.; Luque, A.; Beitia, J. I.; Cano, J.; Lloret, F.; Julve, M.; Alvarez, S. *Inorg. Chem.* **1996**, *35*, 3741–3751. (d) Koga, T.; Furutachi, H.; Nakamura, T.; Fukita, N.; Ohba, M.; Takahashi, K.; Ōkawa, H. *Inorg. Chem.* **1998**, *37*, 989–996. (e) Meyer, F.; Kaifer, E.; Kircher, P.; Heinze, K.; Pritzkow, H. *Chem.—Eur. J.* **1999**, *5*, 1617–1630.

(31) (a) Nanda, K. K.; Das, R.; Thompson, L. K.; Venkatsubramanian, K.; Paul, P.; Nag, K. *Inorg. Chem.* **1994**, *33*, 1188–1193. (b) Nanda, K. K.; Thompson, L. K.; Bridson, J. N.; Nag, K. *J. Chem. Soc., Chem. Commun.* **1994**, 1337–1338. (c) Nanda, K. K.; Das, R.; Thompson, L. K.; Venkatsubramanian, K.; Nag, K. *Inorg. Chem.* **1994**, *33*, 5934–5939.

The magnetic studies reveal that the two nickel(II) ions are ferromagnetically coupled in **2** and antiferromagnetically coupled in **1** and **3**. Preliminary magnetism data in the high temperature range shows that the coupling in **4** is closely similar to that in **3.** To understand the magnetic exchange mechanism, it is important to note the following points, (i) **1** has only one monatomic phenolate-oxygen as bridge, **2** has two monatomic bridges from a phenolate-oxygen and an acetate-oxygen and a *syn*−*syn* μ_2-1, 3-acetate bridge, and **3** has a monatomic phenolate-oxygen plus two *syn*−*syn* μ_2-1,3-acetate bridges; (ii) the values of the Ni−O−Ni angles are 126.19° (**1**), 100.33° (**2**), and 112.78° (**4**); (iii) finally, the intramolecular Ni···Ni distances (Å) for **1**, **2**, and **4** are 3.65 (**1**), 3.12 (**2**), and 3.36 (**4**). For complex **3**, we expect the same structural parameters as those of **4**.[32]

For a series of dinickel(II) macrocyclic complexes of variable stereochemistry, Nag and co-workers demonstrated[31] magneto-structural correlation between the values of J and the Ni−O−Ni bridging angle (and hence Ni···Ni distance), wherein the inversion from ferromagnetic to antiferromagnetic coupling is anticipated at a bridging angle of 97°. This value is quite similar to the value found by Hatfield and co-workers for hydroxyl-bridged dinuclear copper(II) complexes.[33]

Given that, the Ni−O−Ni bond angles of the three dinickel(II) complexes are larger than the critical angle (97°) and taking into account the above comments, an antiferromagnetic coupling through the monatomic bridge is expected for these three complexes. The monatomic bridge is the only exchange pathway for **1**, and its large Ni−O−Ni bridging angle (≈126°) accounts for the strong antiferromagnetic coupling observed.

There are two types of exchange pathways for **2** and **3**, the monatomic and the *syn*−*syn* μ_2-1,3-acetate bridges, which mediate antiferromagnetic exchange pathway. However, it has been shown that the *syn*−*syn* carboxylate and monatomic carboxylate bridges are countercomplementary, and hence the antiferromagnetic contributions of each bridge cancel each other. In **3**, this cancellation is partial, and a very weak antiferromagnetic coupling is observed ($J = -1.24$ cm^{-1}) while in **2** it is total and the ferromagnetic term dominates ($J = +9.80$ cm^{-1}).

Solution-state magnetic susceptibilities on **1**−**4** were obtained by the NMR technique of Evans[13] in CH_2Cl_2. At room temperature the solution state μ_{eff}/Ni values for complexes **1**, **2**, **3**, and **4** are 2.99, 3.15, 3.14, and 3.14 μ_B, respectively. Thus, the solid-state structures are retained in solution.

Redox Properties. To investigate the stability of the mixed-valent $Ni^{III}Ni^{II}$ state for **1**−**4**, cyclic voltammetric (CV) measurements were performed in dichloromethane solutions at a platinum working electrode. All the four complexes display an oxidative response at $E_{1/2}$ values

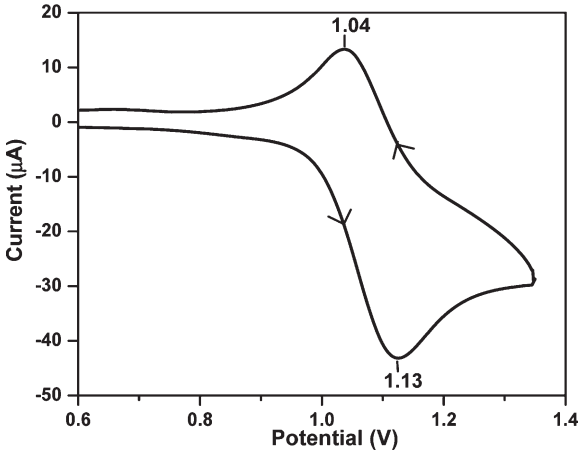

Figure 6. Cyclic voltammogram (scan rate =100 mV/s) of $[Ni^{II}_2(L^1)(O_2CMe)_2(H_2O)_2][PF_6]\cdot MeOH\cdot 3H_2O$ (**1**) in CH_2Cl_2 at a platinum electrode; supporting electrolyte: [^{n}Bu$_4$N][ClO$_4$].

(V vs SCE) of 1.09 (**1**), 1.08 (**2**), 1.17 (**3**), and 1.17 (**4**). An additional redox response could also be seen for **2** at E_{pa} = 0.99 V (Supporting Information, Figure S7) and for **4** at E_{pa} = 0.90 V vs SCE (Supporting Information, Figure S9). Such responses must be associated with coordinated NCS^- oxidation in **2** and BPh_4^- oxidation for **4**. The redox responses are well-behaved for **1** (Figure 6) and **3** (Supporting Information, Figure S8). We tentatively assign this response as due to $Ni^{III}Ni^{II}/Ni^{II}Ni^{II}$ redox process. Similar CV behavior for the phenoxo-bridged dinickel(II) complexes are reported in the literature.[24] All our attempts to investigate the nature of chemical species present in such oxidized solutions failed, as the solutions readily decomposed.

Potentiometric Titrations. To determine the pK_a values of the coordinated water molecules in **1** and **3**,[32] potentiometric titrations were carried out in MeOH−H_2O (33%, v/v; ionic strength was maintained at I = 0.1 M $NaNO_3$) solutions because of the low solubility of these compounds in pure water. Typical curves obtained from the titrations of **1** and **3** with 0.01 N NaOH are shown in Figure 7 and Supporting Information, Figure S10, respectively. It is understandable that the labile ligand (coordinated MeOH) present in the solid of **3** would not remain coordinated and is expected to be replaced by a water molecule, under the experimental conditions. The results obtained for the two complexes show the neutralization of 2 mol of NaOH per mol of the complex in the pH range of 7.5−11. Treating the data, two deprotonation constants were thus obtained for each complex. The distribution curves for **1** and **3** are displayed in Figure 8 and Supporting Information, Figure S11, respectively. The pK_a values of the coordinated water molecules were calculated to be 7.78 ± 0.04 and 8.50 ± 0.04 for **1** and 7.95 ± 0.04 and 8.78 ± 0.03 for **3**.

It has recently been demonstrated that for bis-μ_2-1,3-acetato-bridged dinickel(II) systems supported by endogenous phenolate bridges at pH 9.00 the acetate ions do not remain coordinated to the nickel(II) centers and are replaced by water molecules.[25b] Given this observation and similar observation for closely related systems[34] we

(32) (a) The complex **4** is structurally characterized but not **3**; however, physicochemical studies (cf. electronic spectra, redox properties) show that the cations of these two complexes are identical. (b) It should be mentioned here that because of solubility reasons in 33% MeOH−H_2O mixture (v/v; ionic strength was maintained at I = 0.1 M $NaNO_3$), potentiometric and kinetic experiments were done with complex **3** instead of **4**. Complex **4** was synthesized only to grow single-crystals.

(33) Crawford, V. H.; Richardson, H. W.; Wasson, J. R.; Hodgson, D. J.; Hatfield, W. E. *Inorg. Chem.* **1976**, *15*, 2107–2110.

(34) Lanznaster, M.; Neves, A.; Bortoluzzi, A. J.; Szpoganicz, B.; Schwingel, E. *Inorg. Chem.* **2002**, *41*, 5641–5643.

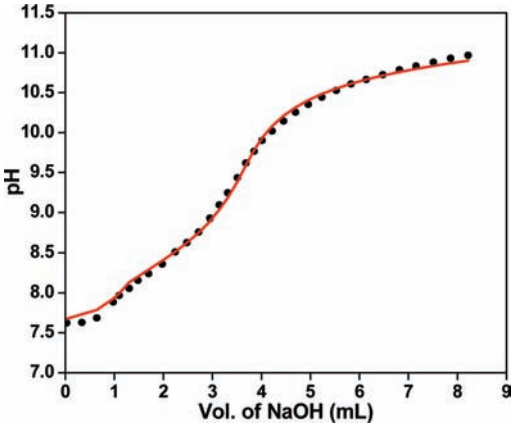

Figure 7. Representative titration curve obtained by titrating $[Ni^{II}_2(L^1)(O_2CMe)_2(H_2O)_2][PF_6]\cdot MeOH\cdot 3H_2O$ (**1**) with 0.01 N NaOH. The experimental points (black dots) are in good agreement with a theoretical curve (red line).

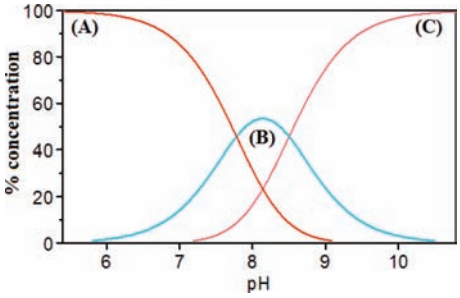

Figure 8. Species distribution curves of $[Ni^{II}_2(L^1)(O_2CMe)_2(H_2O)_2][PF_6]\cdot MeOH\cdot 3H_2O$ (**1**) as a function of pH.

believe that for the complex **3**,[32] at pH 8.50 a similar situation would prevail under the experimental conditions employed in the kinetics experiments of this investigation. Moreover, given the closely similar behavior of the complexes **1** and **3** toward phosphate ester hydrolysis (see below) we are inclined to believe that solution species at a given pH for both the complexes are similar. To throw light on the species composition for complexes **1** and **3** in MeOH−H_2O (33%, v/v) at pH 8.50, such solutions were subjected to positive ESI−MS spectral analysis. The results of complex **1** (Supporting Information, Figure S12) and complex **3** (Supporting Information, Figure S14) indicate generation of solvated species. In fact, complex **1** showed a peak at m/z = 653 corresponding to the species $[Ni^{II}_2(L^1)(MeOH)_2(H_2O)_2(OH)_2]^+$ (species **C**; Scheme 1), based on the simulated mass and isotopic distribution pattern (Supporting Information, Figure S13).[35] For **3** the peaks at m/z 641 and 717 are attributed to the species $\{[Ni^{II}_2(L^2)(MeOH)(H_2O)_4]^{3+} + 2e^-\}^+$ [reduced form of species **A** (Scheme 1), generated during ESI−MS experiment] and $\{[Ni^{II}_2(L^2)(MeOH)(H_2O)_4(OH)]^{2+} + OAc^-\}^+$ (species **B** with an additional acetate ion; Scheme 1), respectively. The isotopic distribution patterns[35] are shown in Supporting Information, Figure S15. The ESI−MS results point to the fact that under the conditions of a hydrolysis experiment the acetate ions are prone to be liberated from

(35) Isotopic distribution pattern was modeled using *Molecular Weight Calculator*, version 6.45; Monroe, M.

Scheme 1

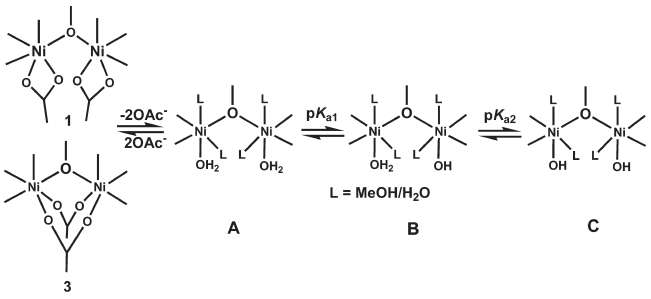

1 and **3**, and hence solvent molecules occupy the vacated sites at the nickel(II) center(s). From this information and in light of the potentiometric titration data (see above), we are inclined to believe that the two pK_a values observed for complexes **1** and **3** are due to the conversion of "$Ni^{II}(H_2O)Ni^{II}(H_2O)$" to "$Ni^{II}(H_2O)Ni^{II}(OH)$" species (p$K_{a1}$) and "$Ni^{II}(H_2O)Ni^{II}(OH)$" to "$Ni^{II}(OH)Ni^{II}(OH)$" species (p$K_{a2}$) (Scheme 1). In essence, we propose the formation of the species "$Ni^{II}(OH)Ni^{II}(OH)$" as the active species during hydrolysis experiments (see below).

It is well-known that the relative acidity of coordinated water molecules is usually associated with the influence of the donor atom *trans* positioned in the coordination sphere of the metal center. The longer the metal-donor atom bond distance, the stronger the metal-water interaction, and lower the observed pK_a value.[25b] The present results do not strictly conform to this generalization. The above trend of the pK_a values of complexes **1** and **3**[32] can be rationalized if one compares the metal−ligand bond lengths between the two complexes. For **1** the average Ni−O_{ph} (ph = phenolate), Ni−N_{py} (py = pyridine), Ni−N_{am} (am = amine), Ni−O_{ac} (ac = acetate) distances are 2.044, 2.060, 2.088, and 2.138 Å, respectively. For **4** the average Ni−O_{ph}, Ni−N_{py}, Ni−N_{pz} (pz = pyrazole), Ni−O_{ac} distances are 2.020, 2.122, 2.027, and 2.034 Å, respectively. It is clear that the ligand $L^2(-)$ binds two Ni^{II} centers more strongly than the ligand $L^1(-)$ does [average metal−ligand bond distances (excluding metal−ligand (solvent) bond lengths) for **1** and **4**[32] are 2.083 Å and 2.051 Å, respectively]. Given these metric parameters (Table 2) it is understandable why average Ni^{II}−OH_2 bond distance is 2.082 Å for **1** and 2.122 Å [Ni−O(H)Me bond distance: 2.131 Å] for **4**.[32] These data clearly justifies why the pK_a values of **1** are lower than that of **3**. Notably, these pK_a values (see above) are low for metal-bound water (cf. the pK_a of $[Ni(H_2O)_6]^{2+}$ is approximately 9.9).[36]

Phosphate Ester Hydrolysis Studies. In recent years a number of investigations have been made to test the potential of dinickel(II) complexes with vacant labile coordination site(s) for the hydrolysis of phosphate esters.[22,25b,37] The catalytically active site of a synthetic hydrolase[25b,38] should be able to (i) provide two labile sites, *cis*-oriented to coordinate the substrate and provide an H_2O/OH^- as the nucleophile, (ii) decrease the pK_a of a

(36) (a) Barnum, D. W. *Inorg. Chem.* **1983**, *22*, 2297–2305. (b) Barrios, A. M.; Lippard, S. J. *J. Am. Chem. Soc.* **1999**, *121*, 11751–11757.

(37) (a) Carlsson, H.; Haukka, M.; Nordlander, E. *Inorg. Chem.* **2002**, *41*, 4981–4983. (b) Carlsson, H.; Haukka, M.; Bousseksou, A.; Latour, J.-M.; Nordlander, E. *Inorg. Chem.* **2004**, *43*, 8252–8262.

(38) Hendry, P.; Sargeson, A. M. *J. Am. Chem. Soc.* **1989**, *111*, 2521–2527. (b) Hendry, P.; Sargeson, A. M. *Prog. Inorg. Chem.* **1990**, *38*, 201–238.

Scheme 2

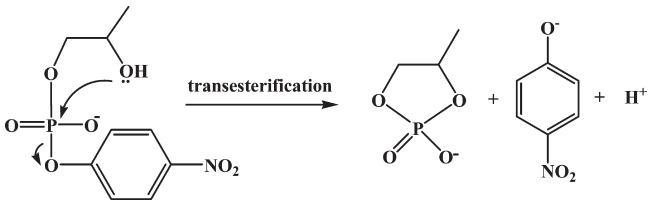

coordinated water molecule, and as a consequence, provide a hydroxide nucleophile coordinated to the metal center at a pH close to neutral, and (iii) activate the substrate through a nucleophilic attack and/or stabilize the transition state, and (iv) release the product(s) at a reasonable rate. The complexes **1** and **3**[32] (cf. crystal structure) have two labile sites for substrate binding and to provide an H_2O/OH^- as the nucleophile, and hence are ideal candidates to explore their potential to catalyze the hydrolysis of an organophosphate ester. To test the activity of complexes **1** and **3** toward phosphate ester hydrolysis, activated phosphoric acid ester 2-hydroxypropyl-*p*-nitrophenylphosphate (HPNP), popularly used as RNA modeling substrate,[6e,g] is used. HPNP releases *p*-nitrophenolate by intramolecular nucleophilic attack of the appended hydroxide group and formation of a cyclic phosphodiester (Scheme 2). The formation of cyclic phosphodiester product has been authenticated by ^{31}P NMR spectroscopy. The hydrolysis of HPNP by complex **1** was monitored by a time-dependent ^{31}P NMR spectral study. ^{31}P NMR spectra obtained, under conditions of excess substrate (see above), at various time intervals are given in Supporting Information, Figure S16. The chemical shift of HPNP is at −5.17 ppm. As the hydrolysis reaction proceeds, the formation of the cyclic phosphodiester is observed at 17.98 ppm.[19] At longer times (t = 18 h) almost all the substrates are hydrolyzed to cyclic phosphodiester.

To investigate the phosphatase-like activity[6a,e,g,22,25b,37] experiments have been carried out by monitoring spectrophotometrically the absorption increase of the liberated *p*-nitrophenolate anion [λ_{max} = 400 nm with ε = 18 500 M^{-1} cm^{-1}; considering equilibration *p*-nitrophenol/*p*-nitrophenolate (pK_a = 7.15)],[18] under pseudo first-order conditions (excess complex). In the first set of experiments, the pH dependence of the catalytic activities was investigated in the pH range 7.00−10.00 and 7.50−10.00, for complexes **1** and **3**, respectively. As shown in Figures 9 and Supporting Information, Figure S17, the rates versus pH plots for the two complexes have sigmoidal shapes, characteristic of a kinetic process controlled by an acid−base equilibrium. The experimental data reveals that the rate is highly influenced by pH of the medium, the reaction rate increases with increase in pH, and finally gets saturated at higher pH. These curves were simulated by the Boltzman model[39] and the kinetic pK_a values determined (complex **1**, pK_a 8.64 ± 0.02; complex **3**, pK_a 8.75 ± 0.03). These values are in reasonable agreement with the pK_{a2} values determined by potentiometric titration (pK_{a2}: 8.50 ± 0.04 for **1**; pK_{a2}: 8.78 ± 0.03 for **3**). A closely similar situation was observed by Greatti et al.[25b] The excellent agreement between the kinetic and the potentiometric pK_a values reinforces the proposal that deprotonation of a coordinated water molecule is necessary to generate the catalytically active Ni^{II}-coordinated hydroxo species "$Ni^{II}(OH)Ni^{II}(OH)$" (Scheme 1).

(39) A computer simulation (sigmoidal curve fitting, Origin version 6.0) of the dependence of rate of a reaction on pH was performed using the Boltzman equation: $y = (A_1-A_2)/\{1 + \exp(x-x_0)/dx\} + A_2$, where A_1 = upper rate value; A_2 = lower rate value; x = pH; $x_0 = pK_a$.

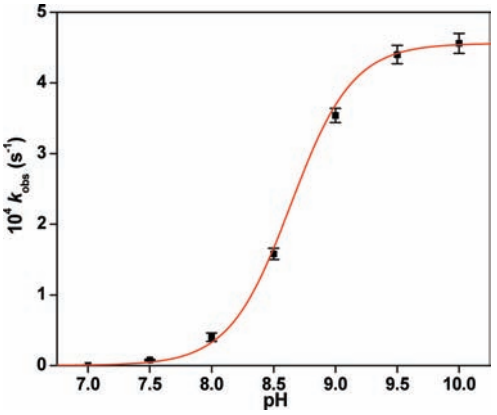

Figure 9. Dependence of the rate (k_{obs}) on pH for the hydrolysis of HPNP promoted by complex $[Ni^{II}_2(L^1)(O_2CMe)_2(H_2O)_2][PF_6]\cdot MeOH\cdot 3H_2O$ (**1**). [Complex] = 50×10^{-5} M; [HPNP] = 5×10^{-5} M; [buffers] = 20×10^{-3} M; I = 0.1 M ($NaNO_3$) in MeOH−H_2O (33%, v/v) at 30 °C.

The hydrolysis reaction of HPNP by complexes **1** and **3** has been investigated, under pseudo first-order conditions (excess complex concentration at pH 8.50 and at 30 °C). The time-course of the change in the absorbance for the hydrolysis of HPNP by compound **1** at different concentrations is shown in Figure 10. The kinetics data reveal that for both complexes the rate of the hydrolysis is linearly dependent on the concentration of complexes **1** and **3** (Figure 11 and Supporting Information, Figure S18 for **1** and **3**, respectively), and the following second-order rate constants (k_2) were calculated from the slope of the straight lines of k_{obs} versus [complex]: k_2 = 0.30 M^{-1} s^{-1} for **1** and k_2 = 0.058 M^{-1} s^{-1} for **3**. It is important to note that complex **1** is more reactive than complex **3** (Table 3). No significant hydrolysis of the test substrate occurred when the metal complex was absent. Interestingly, the values of the second-order rate constants for both the complexes are slightly lower than but comparable to the catalytic efficiency values k_{cat}/K_M (0.42 M^{-1} s^{-1} for **1** and 0.089 M^{-1} s^{-1} for **3**), obtained from the kinetic studies under Michaelis−Menten conditions (Supporting Information, Table S1).

Understandably, for any complex to act as an efficient catalyst for hydrolysis of the substrate the incoming substrate should first get bound effectively to the catalyst, which is dictated by a combination of geometrical and electronic factors of the metal−ligand unit. This event should be followed by attack of the metal-coordinated hydroxide nucleophile to the substrate. The greater ability of the dinickel(II) center in **1** compared with **3** to hydrolyze HPNP could be due to stronger electron donating effect of $L^2(-)$ in **3** than $L^1(-)$ in **1** (cf. comparison of metal−ligand metric parameters; see above). This in turn is expected to control the Lewis acidity of coordinated water (see above). Moreover, the relative orientation

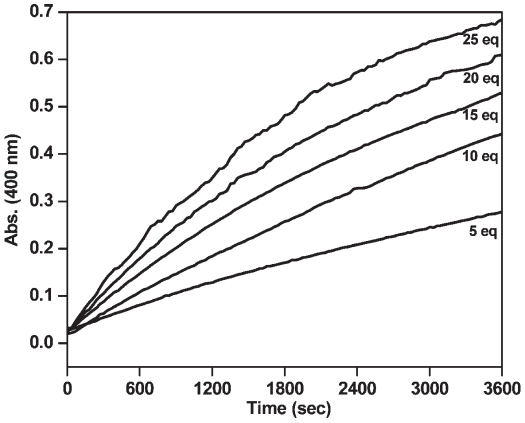

Figure 10. Time-course for the change in the absorbance for the hydrolysis of HPNP by the complex $[Ni^{II}_2(L^1)(O_2CMe)_2(H_2O)_2][PF_6]\cdot MeOH\cdot 3H_2O$ (**1**). Conditions: [HPNP] = 5×10^{-5} M; [complex] = 25×10^{-5} to 125×10^{-5} M; buffer CHES (pH 8.50), $I = 0.1$ M ($NaNO_3$) in MeOH−H_2O (33%, v/v) at 30 °C.

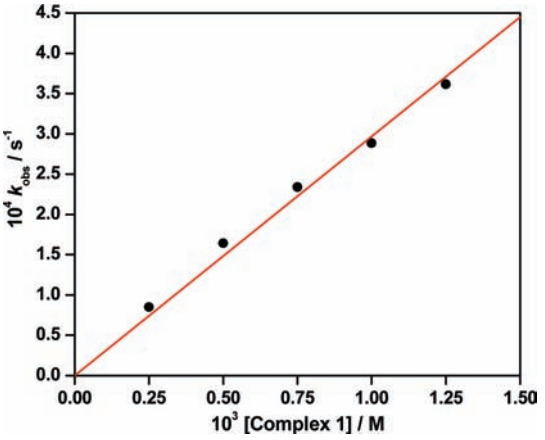

Figure 11. Dependence of the reaction rate on the concentration of the complex $[Ni^{II}_2(L^1)(O_2CMe)_2(H_2O)_2][PF_6]\cdot MeOH\cdot 3H_2O$ (**1**) for the hydrolysis of HPNP. Conditions: [HPNP] = 5×10^{-5} M; [complex] = 25×10^{-5} to 125×10^{-5} M; buffer CHES (pH 8.50), $I = 0.1$ M ($NaNO_3$) in MeOH−H_2O (33%, v/v) at 30 °C.

of Ni^{II}-coordinated hydroxide nucleophile with respect to HPNP binding is expected to play an important role for subsequent attack by active species "$Ni^{II}(OH)Ni^{II}$-(OH)" (species **C**; Scheme 1) to the bound substrate. Given the enhanced flexibility of $L^1(-)$ (six-membered chelate ring) it is reasonable to assume that the nucleophilic attack by the active species to Ni^{II}-bound HPNP would be favorable for complex **1** over complex **3** (five-membered chelate ring). Furthermore, at pH 8.50 complex **1** has approximately 46% of the active species "$Ni^{II}(OH)Ni^{II}(OH)$", whereas complex **3** contributes only 29%. The higher catalytic efficiency of **1** compared to **3** toward HPNP hydrolysis could be due to higher effective concentration of the active species.

To investigate the influence of acetate ion on the rate of hydrolysis of HPNP by complexes **1** and **3**, the hydrolysis reaction was monitored as a function of acetate concentration, under the experimental conditions employed in the kinetic experiments. Supporting Information, Figure S19 shows the percentage of inhibition on the hydrolysis reaction versus number of acetate equivalents added. It is obvious that the acetate ion inhibits the hydrolysis reaction. When the acetate concentration equals the substrate concentration, a reduction of the rate by 30% for **1** and by 25% for **3** is observed. With addition of 20 equiv of acetate ion such values reach 50% for **1** and 42% for **3**. These results support the finding (see above) that the acetate ions are prone to be released during hydrolysis experiment. Hence acetate ion can be considered as inhibitors for this reaction when present in high concentration. A similar situation was also observed by Greatti et al.[25b]

The dependence of temperature (30−45 °C) on the rate of hydrolysis of HPNP by complexes **1** and **3** was also investigated, under the experimental conditions employed in the kinetics experiments. The activation energies and parameters E_a, $\Delta H^{\ddagger}$, $\Delta S^{\ddagger}$, and $\Delta G^{\ddagger}$ (Table 4) were obtained through the Arrhenius and the Eyring equations. Figures 12 and Supporting Information, Figure S20 show the linearization of the observed rate constants (k_{obs}'s) for the reactions catalyzed by complexes **1** and **3**, respectively. Unfortunately, there are no reports of activation parameters

Table 3. Observed Pseudo First-Order Rate Constants for Hydrolysis/Transesterification of HPNP in MeOH−H_2O (33%, v/v) Buffer CHES at pH = 8.50, I = 0.1 M ($NaNO_3$), 30°C with [catalyst] = 50×10^{-5} M and [HPNP] = 5×10^{-5} M

catalyst	k_{obs} [10^{-5} s^{-1}]	k_{obs}/k_{uncat}
1	16.50	730
3	2.96	130
uncatal	0.0226	1

for the hydrolysis of HPNP by any phenoxo-bridged dinickel(II) complex. Therefore, no comparisons of the obtained activation parameters can be made. However, the following comments are in order. Notably, in both cases $\Delta S^{\ddagger} < 0$, indicating that an organization of the reactive species occurs in the transition state. Also in both cases, $\Delta H^{\ddagger} > 0$, reflecting bond breaking in the activated complex. The activation energy for the reaction carried out in the presence of complex **1** is lower than that obtained for complex **3**. This is in agreement with the observed reaction rates. The data in Table 4 point toward the conclusion that the hydrolysis of HPNP promoted by complexes **1** and **3** occurs through a similar mechanism.

Finally, the following comments on the hydrolysis of phosphate esters by metallohydrolases in general and hydrolysis of HPNP by synthetic dimetal(II) complexes [in the present case dinickel(II) complexes] in particular are in order. The mechanism of the metal ion-catalyzed hydrolysis of phosphate esters involves,[6a,d,g] as a crucial initial step, the coordination of the substrate to the metal center(s). This coordination is an essential requisite to deliver the metal ion-coordinated hydroxide nucleophile close to the phosphate group. This offsets the electrostatic repulsion between the two negatively charged species (substrate and the nucleophile) and allows the activation of the phosphate toward the nucleophilic attack. This would create a double Lewis acid activation for the transesterification reaction.[6a,d,g] It should be mentioned here that although a large number of studies on HPNP transesterification have been reported, a definitive assessment of the mechanism of the reaction assisted by metal ions has not still been made.[6g] Two kinetically

Table 4. Activation Parameters for the Hydrolysis of HPNP

complex	E_A, kJ·mol^{-1}	A, s^{-1} (frequency factor)	$\Delta H^{\ddagger}$, kJ mol^{-1}	$\Delta S^{\ddagger}$, J mol^{-1} K^{-1}	$\Delta G^{\ddagger}$,[a] kJ mol^{-1}
1	67	6.44×10^7	64	−104	95.5
3	71	3.75×10^7	68	−109	101

[a] $\Delta G^{\ddagger} = \Delta H^{\ddagger} - T\Delta S^{\ddagger}$, at 30 °C.

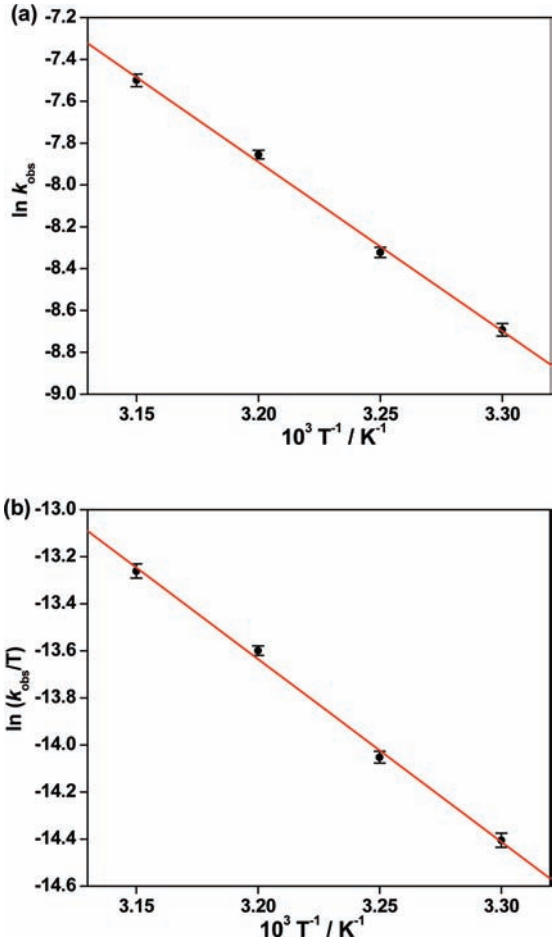

Figure 12. Linearizations of the observed rate constants for the hydrolysis of HPNP (5×10^{-5} M) promoted by complex $[Ni^{II}_2(L^1)(O_2CMe)_2(H_2O)_2][PF_6]\cdot MeOH\cdot 3H_2O$ (**1**) (50×10^{-5} M) as a function of temperature: (a) Arrhenius equation and (b) Eyring equation. Conditions: [buffer] = 20×10^{-3} M (CHES, pH = 8.50); I = 0.1 M ($NaNO_3$) in MeOH−H_2O (33%, v/v).

indistinguishable mechanisms are generally proposed for both mono- and bimetallic systems. The first involves deprotonation of the substrate hydroxyl group by a metal-bound hydroxide, which acts as a general base catalyst. The second possible pathway implies the direct coordination of the substrate's alcoholic function to the metal ion and subsequent nucleophilic attack on the phosphorus center. The pH-rate profile of **1** and **3** clearly demonstrates that this effect alone does not provide sufficient rate acceleration. This would need the concerted action of the double Lewis acid activation and the intramolecular general base catalysis by a metal-bound hydroxide ion (Scheme 3). The organic phosphate ester coordinates to the dinickel(II) complex, possibly bridging through the phosphate group. Direct coordination to the dinickel complex activates the P−O bond for nucleophilic attack.

Scheme 3

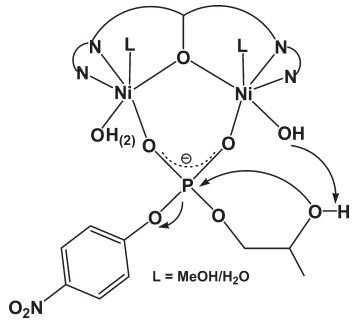

Summary and Concluding Remarks

With the goal to make phenoxo-bridged dinickel(II) complexes supported by (pyridin-2-yl)ethylamine and 3-(pyridin-2-yl)pyrazole units as terminal coordinating units, four complexes, $[Ni^{II}_2(L^1)(O_2CMe)_2(H_2O)_2][PF_6]\cdot MeOH\cdot 3H_2O$ (**1**), $[Ni^{II}_2(L^1)(O_2CMe)_2(NCS)]$ (**2**), $[Ni^{II}_2(L^2)(O_2CMe)_2(MeOH)(H_2O)][ClO_4]$ (**3**), and $[Ni^{II}_2(L^2)(O_2CMe)_2(MeOH)(H_2O)][BPh_4]\cdot 3MeOH\cdot H_2O$ (**4**) have been synthesized, and their physicochemical properties have been studied. The crystallographic analyses of **1** and **4** reveal that in **1** the acetate ions coordinate as bidentate chelating mode while in **4** the acetate ions bind in μ_2-1,3-bidentate bridging mode. While the crystal structure of **3** could not be determined, it is assumed that structural parameters of **3** are closely similar to that of **4**. This contention is supported by closely similar physicochemical properties of **3** and **4**. The X-ray structure of complex **2** was reported previously,[7] but without physicochemical properties. In this work such studies have been completed. This work provides the first magneto-structural characterization of three closely similar phenoxo-bridged dinickel(II) complexes (**1**−**3**), with or without additional acetate bridging. The coordination of water or a methanol molecule to the dinuclear center is very interesting with respect to the discussion of the nucleophilic species in the catalytic hydrolysis/transesterification reactions of HPNP. The two Ni^{II} ions act in concert to lower the pK_a of a coordinated water molecule enough such that it will be deprotonated under physiological conditions (pH≈7). Complex **1** showed higher activity compared to complex **3**. Temperature-dependent measurements were done to evaluate kinetic/thermodynamic parameters for the hydrolysis/transesterification reaction of HPNP and to propose a mechanistic pathway. Our results strengthen the hypothesis that nickel(II) bound hydroxide ion serves as the nucleophile for phosphate ester hydrolysis, and the coordination of the substrate to the dinuclear nickel(II) center is crucial to hydrolysis. The observed result suggests a concerted action of the Lewis acid activation provided by the dinickel(II) core and the intramolecular general base hydrolysis provided by a Ni^{II}-bound hydroxide ion. The promising rate enhancements observed here have stimulated ongoing investigations of hydrolytic properties of complexes, not only Ni^{II} but also

Cu^{II}/Zn^{II}, formed by the 2,6-substituted-phenolate-based dinucleating ligands with varied terminal donor sites.

Acknowledgment. This work is supported by grants from the Department of Science and Technology, Government of India, New Delhi. S.M. gratefully acknowledges the award of SRF by Council of Scientific & Industrial Research, Government of India. Comments of the reviewers were very helpful at the revision stage.

Supporting Information Available: Absorption spectra of **1**−**4** (Figures S1−S4); $\chi_M T$ versus T plot for **3** (Figure S5); χ_M versus T plot for **1** (Figure S6); CV of **2**−**4** (Figure S7−S9); potentiometric titration curve of **3** (Figure S10); species distribution curve of **3** (Figure S11); mass spectral results of **l** and **3** under hydrolysis conditions (Figure S12−S15); ^{31}P NMR spectra of the product of HPNP hydrolysis by complex **1** at different time intervals (Figure S16); dependence of the reaction rate (k_{obs}) on pH for the hydrolysis of HPNP by **3** (Figure S17); dependence of the reaction rate on the concentration of **3** for the hydrolysis of HPNP (Figure S18); percentage inhibition of the hydrolysis reaction of HPNP substrate with acetate catalyzed by **1** and complex **3** (Figure S19); linearizations of the observed rate constants for the hydrolysis of HPNP promoted by **3** as a function of temperature: Arrhenius equation and Eyring equation (Figure S20); kinetic studies of the hydrolysis of HPNP by complexes **1** and **3** under Michaelis−Menten condition: dependence of the initial reaction rate on the HPNP concentration for the hydrolysis reaction by **1** (Figure S21) and **3** (Figure S23); Lineweaver−Burk plot for HPNP hydrolysis catalyzed by **1** (Figure S22) and **3** (Figure S24); kinetic parameters obtained from Lineweaver−Burk plots (Table S1). This material is available free of charge via the Internet at http://pubs.acs.org.